Frictional Compliance Model Development and Experiments for Snake Robot Climbing

Amir Shapiro, Aaron Greenfield, Howie Choset

Abstract— **Intelligently utilizing the frictional contact between a robot and its environment can prevent slip, maintain balance, and provide stability during a robot's motion. A contact model is first needed to enable robot control achieving these goals. The model should be both accurate and simple enough to allow further system analysis. In this paper we propose a simple parametric contact model, based on the form of the Hertz-Walton model. We experimentally demonstrate that this contact model can be effectively used to predict contact forces for linear and near-linear loading paths. Finally, we briefly discuss the applicability of the presented contact model for snake robot climbing. The control of the snake robot is based on stabilizing a sequence of set points.**

I. Introduction

We are interested in snake robot climbing. Already, our group has constructed a snake robot and develop behaviors for it to climb in isolated situations (See Figure 1). Understanding why this seemingly easy demonstration works has proven to be quite difficult. This problem is complex because of the many degrees of freedom the robot has, its energetics, and its contact with the environment, just to name a few challenges. This paper solely focuses on modeling the contact, which is sometimes overlooked in other robotic climbing papers. While this paper does not directly produce generic behaviors for snake robot climbing, the modeling, put forth here, furthers our understanding of contact, which will prove to be useful for future work in robotic climbing.

A climbing task requires both slip prevention and stability. In our climbing experiments it was identified that there must be a compliant material at the contacts to practically allow the robot to climb, thus necessitating a compliant contact model. Moreover, in order to successfully control a robot which is in frictional contact with its environment, we first need models of the contact interaction. Ideally, a contact model would be both accurate enough to capture all the relevant physics of interaction, broad enough to apply in a wide range of contact conditions, and simple enough so that control decisions can tractably be made on the basis of the contact model. In practice, the physics of contact is difficult to model, particularly with computationally tractable models. Lumped parameter models, such as the Hertz model [1] and Walton model [2], attempt to model the contact forces using a small number of state variables like normal and tangential displacements, in order to provide simplicity. However, due to the many complicating factors in predicting contact force, such as hysteresis, energy loss, and microslip, these simple models invariably sacrifice accuracy for simplicity.

A. Shapiro is with Department of Mechanical Engineering, Ben Gurion University of the Negev, P.O.Box 653 Beer-Sheva 84105, Israel ashapiro@bgu.ac.il

A. Greenfield and H. Choset are with the Robotics Institute, Carnegie Mellon University, 5000 Forbes Ave. Pittsburgh, PA 15213, USA {algaei,choset+}@cs.cmu.edu

Fig. 1. Our newly developed snake robot climbing between two walls

In this paper, we develop a parametric model, based on the Walton model, and we experimentally explore the level of accuracy of the model in predicting contact forces. Our model generalizes the Walton model in two fundamental ways. First, our model is not restricted only to linear loading profiles, and can be extended to near-linear loading paths, as experiments show. Second, our model is not only for the case where two identical spheres contacting each other, but also for the contact of a sphere with a plane.

We experimentally look at the accuracy of the contact model in three categories of loading paths. The first category is a normal, or Hertzian loading path. This loading path only involves normal forces, and serves as a comparatively simple first test of the model's accuracy. The second category is linear loading paths in which the compliant material is deflected by a constant ratio of tangential to normal deflections. A variety of deflection ratios are explored to determine the generality of the model. The category of linear loading paths was chosen because it was used by Walton for the derivation of his contact model, which forms the basis of our contact model. Finally, we relax the linearity restriction on the paths, to explore how well the model can generalize to simple non-linear loading paths. This is important because many loading paths may have some deviation from linearity.

II. Related Work

The work of Hertz [1] is one of the earliest and most widely known theories in elastic contact mechanics. Hertz

restricts his attention to the normal loading of two elastic solids, under the assumptions that the contact area is elliptical, and small in comparison to the radii of curvature and the size of the contacting bodies. Since the snake robot uses frictional contacts we are interesting in tangential loading as well as normal loading. Thus, the normal loading assumption is overly restrictive for the contact conditions we consider.

The work of Walton [2], [3] develops the force-displacement relationships used as a basis for the model considered in this paper. Walton considers the oblique loading of two identically shaped spheres, under the assumptions that the spheres are loaded with a constant ratio of normal to tangential displacements, that there is no slip while loading, and that certain energy flow requirements are satisfied. The last is a necessary condition in order to assure uniqueness of solution to the contact equations. As with Hertz, the work of Walton assumes small displacements. A more recent paper by Elata [4] critiques Walton's model by pointing out the thermodynamic inconsistency of this model and noting that there exist closed loop paths which generate energy. Despite the obvious physical impossibility of this phenomenon, the Walton model remains attractive due to its simplicity. Furthermore, the addition of an equivalent damping term to the quasi-static Walton model which dissipates energy would alleviate the thermodynamic inconsistency. However, modeling of equivalent damping is beyond the scope of this paper.

Besides the Walton model, a variety of other models exist which predict both normal and tangential force of contacting bodies [5], [6], [7], [8], [9]. These models are unattractive for our purposes, because we are seeking a simple model that will provide analytical insight on the stability of climbing snake robots. All this work is analytical and based on assumptions which may not hold true in practice due to finite displacements, or other violations of modeling assumptions. It is therefore useful to *experimentally* validate the use of these contact models. The work of Burdick et. al. [10] describes a high fidelity experimental setup which is used to test the validity of the Hertz model for fixturing applications.

III. Compliant Contact Model

The parametric model in this paper is based on the lumped parameter model derived by Walton [2]. The Walton model is based on (but not only) the following assumptions: First, the contact force is within its friction cone (i.e. no slippage occur). Second, the loading path is linear, that is, there exist constant ratio between the normal and the tangential deflections. Third, the two contacting bodies are identically shaped spheres with equal material properties. Under these assumptions Walton developed the pressure-displacement model as

$$\begin{bmatrix} q_n \\ q_t \end{bmatrix} = \begin{bmatrix} \frac{4G}{\pi R(1-\nu)}\sqrt{(R_1^2 - r^2)} \\ \frac{8G\delta_t}{\pi R_1^2(2-\nu)}\sqrt{(R_1^2 - r^2)} \end{bmatrix} \quad (1)$$

where q_n is the normal pressure (i.e. normal force per unit of the contact area), q_t is the tangential traction (i.e. tangential force per unit of the contact area), G is the shear modulus,

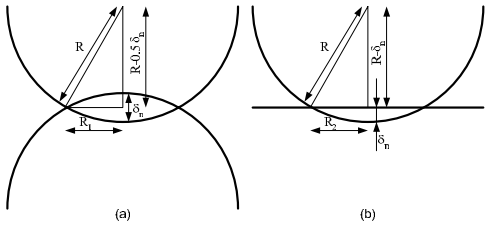

Fig. 2. (a) R_1 is the radius of the contact area between the two identical spheres, and (b) R_2 is the contact area radius between a sphere and a plan

ν is the poisson ratio, R is the common sphere radius, $R_1 = \sqrt{R\delta_n}$ is the contact area radius, and r is the distance from the center of the contact patch which has a disc shape. The normal deflection, δ_n, is defined as the minimum amount of translation needed to separate the contacting bodies. The tangential deflection, δ_t, is being accumulated along the loading path as follows: at every instance during the loading we take the projection of the loading velocity along the tangential direction, and integrate it over the time period of the loading and unloading.

The pressure-displacement model can be integrated over the contact area yields the force displacement relationship

$$\begin{bmatrix} f_n \\ f_t \end{bmatrix} = \begin{bmatrix} \int_0^{\sqrt{R\delta_n}} q_n 2\pi r dr \\ \int_0^{\sqrt{R\delta_n}} q_t 2\pi r dr \end{bmatrix} = \begin{bmatrix} \frac{8G\sqrt{R}}{3(1-\nu)}\delta_n^{\frac{3}{2}} \\ \frac{16G\sqrt{R}}{3(2-\nu)}\sqrt{\delta_n}\delta_t \end{bmatrix} \quad (2)$$

where f_n, f_t are the normal and tangential contact forces respectively. Note that in this case the deflection ratio $\frac{\delta_n}{\delta_t}$ is held constant throughout the loading process.

The underlying assumptions of the Walton model are not valid for snake robot climbing because climbing involves contact between an *elastic sphere and a comparatively rigid plane*. In particular, the radius of the circular Hertzian contact area between two identical spheres, $R_1 = \sqrt{R\delta_n}$, used in Walton's derivation to integrate the traction distribution is no longer valid. It is important at this point to explain how Hertz derived this contact area radius. From Figure 2 (a) one can see using simple geometry that R_1 must satisfy the Pythagoras equation $R_1^2 + (R - \frac{1}{2}\delta_n)^2 = R^2$. Solving this equation for R_1 while neglecting high order terms of δ_n yields the Hertzian contact area radius.

For a sphere on a plane, the geometry of our experiments, we can derive the radius of the new Hertzian contact area using plane geometry as shown in the Figure 2 (b). In this case the Pythagoras equation requires that R_2 must satisfy is $R_2^2 + (R - \delta_n)^2 = R^2$. Applying the same procedure as before yields the new contact area radius as $R_2 = \sqrt{2R\delta_n}$. Integrating Walton's normal pressure and tangential traction over the new contact area yields the lumped parameter model to be used for our experiments as

$$\begin{bmatrix} f_n \\ f_t \end{bmatrix} = \begin{bmatrix} \int_0^{\sqrt{2R\delta_n}} q_n 2\pi r dr \\ \int_0^{\sqrt{2R\delta_n}} q_t 2\pi r dr \end{bmatrix} = \begin{bmatrix} \frac{16\sqrt{2}G\sqrt{R}}{3(1-\nu)}\delta_n^{\frac{3}{2}} \\ \frac{16\sqrt{2}G\sqrt{R}}{3(2-\nu)}\sqrt{\delta_n}\delta_t \end{bmatrix}. \quad (3)$$

This is the parametric model that we wish to experimentally validate in this paper, and which we fit to the force-

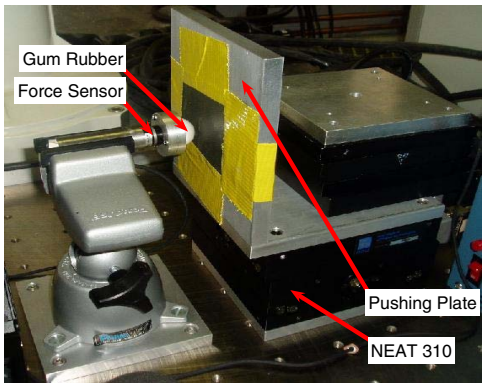

Fig. 3. Experimental setup showing the compliant material, a gum rubber, mounted to a static force sensor which is clamped to an experimental table. A two-axis displacement device NEAT 310 drives the pushing plate into the compliant material.

displacement data in subsequent sections is

$$\begin{bmatrix} f_n \\ f_t \end{bmatrix} = \begin{bmatrix} k_n \delta_n^{\frac{3}{2}} \\ k_t \sqrt{c} \delta_t^{\frac{3}{2}} \end{bmatrix} \tag{4}$$

where c is the deflection ratio $c = \frac{\delta_n}{\delta_t}$, and k_n, k_t are constants that lump the material and geometric properties of the contacting bodies as appear on (3).

The resultant model in (4), which is more applicable to our experiment than the original Walton model, still has the same functional dependence on displacements as the Walton model. In our experiments, we only seek to validate this models dependence on displacements so the simplified form listed in (4) is all that is necessary in subsequent sections.

IV. Experiments and Results

The purpose of the experiments is to determine how effectively the simple lumped parameter model in (4) can be used to predict contact forces. In particular, we would like the model to be valid for a variety of loading paths, including normal loading paths, linear loading paths, and some range of non-linear loading paths as well.

A. Experimental Setup

The three main components of our experimental setup, required to generate force-displacement data, are a high precision displacement device, a force sensor, and the compliant material. The overall setup is shown in Figure 3.

We utilized the NEAT-310, produced by New England Affiliated Technologies, as a high precision displacement devise. The NEAT-310 consists of a two axis output stage, with each axis individually driven by a $1[\mu m]$ resolution stepper motor. The force sensor we used was the Nano17 6-axis force-torque sensor by ATI Industrial Automation. The force resolution of the device is $\frac{1}{1280}[N]$ on each force axis and is rated up to $50[N]$. The compliant material we chose to experiment on was a pure gum rubber ball available from McMaster-Carr as part number 96385K62. This material was chosen primary for its compliance properties, which rates it as a 45-50 on the Shore A scale[1]. The material is sold as a 1" diameter ball. The main advantage of using such a compliant material is that the compliance of the rest of the system (i.e. force sensor and structural compliance) is negligible with respect to the compliance of the rubber ball.

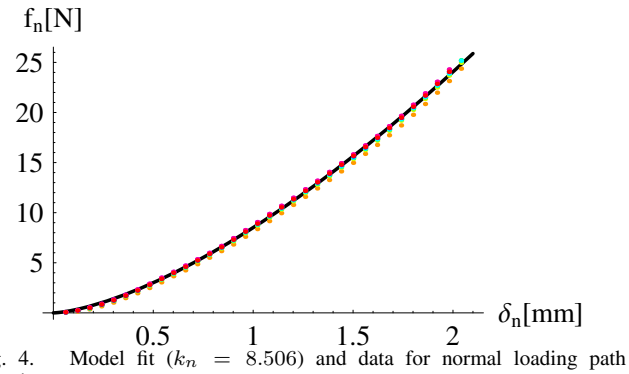

Fig. 4. Model fit ($k_n = 8.506$) and data for normal loading path experiments

In order to setup the three main components, the compliant material was cut in half to make a half-sphere, and mounted onto a plate which attached to the force sensor. The force sensor was screwed to an aluminum tube, which was clamped and then the clamp was screwed to an experimental table. This setup held the compliant material fixed with respect to the experimental table. The NEAT-310 stage was also screwed to the experimental table. A vertical aluminum plate was attached to the device's output stage. This vertical plate, covered with sandpaper to increase contact friction, served as the pushing surface to compress the complaint material. See Figure 3.

B. Normal Loading Path Experiments

Ten normal loading experiments were conducted, each of which loaded the compliant material to 25 [N] in the normal direction. The normal component of the parametric model in (4) was then fit to this data. The tangential component could not be estimated based on these experiments, since no tangential deflection was produced. The results of the ten experiments, as well as the fit model are shown in Figure 4.

In order to assess the quality of the fit, which visually appears accurate, statistics were generated and are shown in Table I. All statistical quantities used in the paper are defined in the Appendix. The model appears to fit the normal loading path data well.

TABLE I
Normal Loading Path Statistics

R^2	Mean Abs. Err.	Mean Norm. Abs. Err.	Max Err.	Min Err.
.9997	.1677[N]	3.421%	.7523[N]	-.8248[N]

[1]Shore A is a scale for measuring Durometer hardness which is the international standard for measuring the hardness of rubber, plastic, and most nonmetallic materials. For the intuition sake, 40 on Shore A scale corresponds to the hardness of common pencil eraser

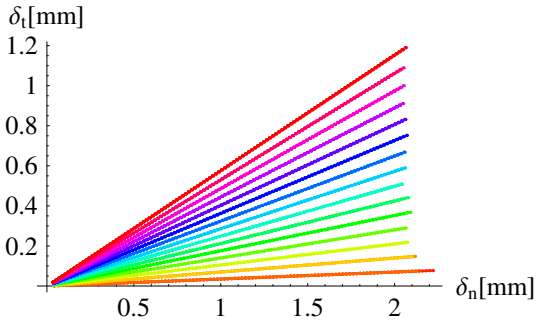

Fig. 5. Loading paths for the linear loading experiments

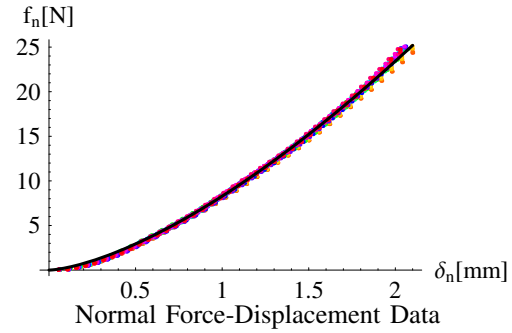

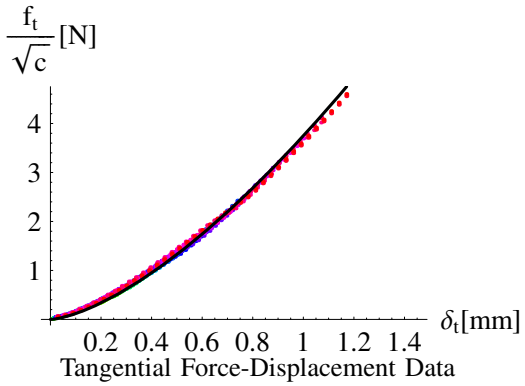

Fig. 6. Normal and Tangential Component Model fit and data ($k_n = 8.280, k_t = 3.7482$) for linear loading path experiments

C. Linear Loading Path Experiments

Forty-five linear loading path experiments were performed. In each experiment, the pusher compressed the compliant material at a constant ratio between normal and tangential deflection. The material was compressed at fifteen different angles in the (δ_n, δ_t) plane ranging from two degrees to 30 degrees in increments of two. Each angle was repeated three times. See Figure 5 for the loading paths used in the experiments. Each experiment was run until there was a 25[N] force in the normal direction.

The results of the experiments, along with the fit to the data, is shown in Figure 6. In the tangential direction, we have normalized the force by the square root of the ratio of deflections used in each particular experiment, $\sqrt{c} = \sqrt{\frac{\delta_n}{\delta_t}}$. The reason for this is to visualize the data solely as a function of δ_t and not δ_n, recall from (4) that $f_t/\sqrt{c} = k_t \delta_t^{3/2}$.

To assess the quality of the fit we again generate several statistics, independently for the fit in the normal direction and the tangential direction. The statistics are shown in Table II. Again the fit appears quite good, indicating that our parametric model can adequately predict linear loading path experimental data. This is significant because our experiments violate the small deflection assumption of this model as well as the assumption that two uniformly shaped spheres are in contact. Additionally, the parameter k_n agrees closely with the value fit from the normal loading paths. This is not unexpected, since a normal loading is also a linear loading path.

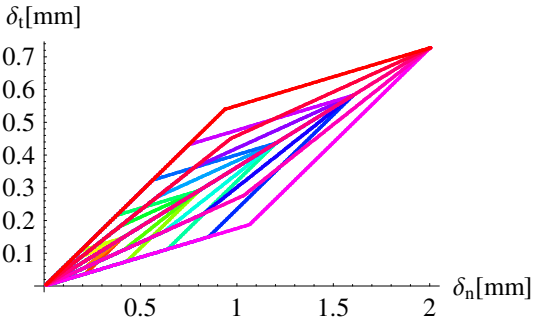

Fig. 7. Loading path experiments for nonlinear loading Set 1. The five convergence points are the five points on the linear loading path where the loading paths converge together.

TABLE II

TANGENTIAL LOADING PATH STATISTICS,NORMAL & TANGENTIAL FITS

	R^2	Mean Abs. Err.	Mean Norm. Abs. Err.	Max Err.	Min Err.
Normal	.9993	.2326[N]	5.21%	1.187[N]	-2.241[N]
Tan.	.9982	.0482[N]	13.02%	.1439[N]	-.2036[N]

D. Nonlinear Loading Path Experiments

One hundred and fifty nonlinear loading path experiments were performed, in three sets of fifty, which we denote Set 1,2, and 3. Each nonlinear experiment consisted of two linear segments. In each set of fifty experiments, five points in the (δ_n, δ_t) plane were chosen, equally spaced along linear loading path at 20 degrees, which we term *convergence points*. Five different loading paths converged on each of these five points at different angles, and each loading path was repeated twice, for a total of fifty experiments. See Figure 7 for the loading paths used in Set 1 experiments. The convergence points in this figure are the common points where the paths intersect.

In the nonlinear loading Set 1 experiments, the approach angle ranged from 10 to 30 degrees in increments of five degrees. In the Set 2 experiments, the approach angles ranged from 16 to 24 Degrees in increments of two degrees, and finally in the Set 3 experiments, the approach angle ranged from 18 to 22 degrees in increments of 1 degree. Therefore the nonlinear loading experiments become closer to linear paths as we move from Set 1 to Set 3.

The data points from all loading paths at the loading path convergence points are shown in Figure 8 along with fits to the linear loading path data in each experiment set. The data appears linear in the (f_n, f_t) plane due to

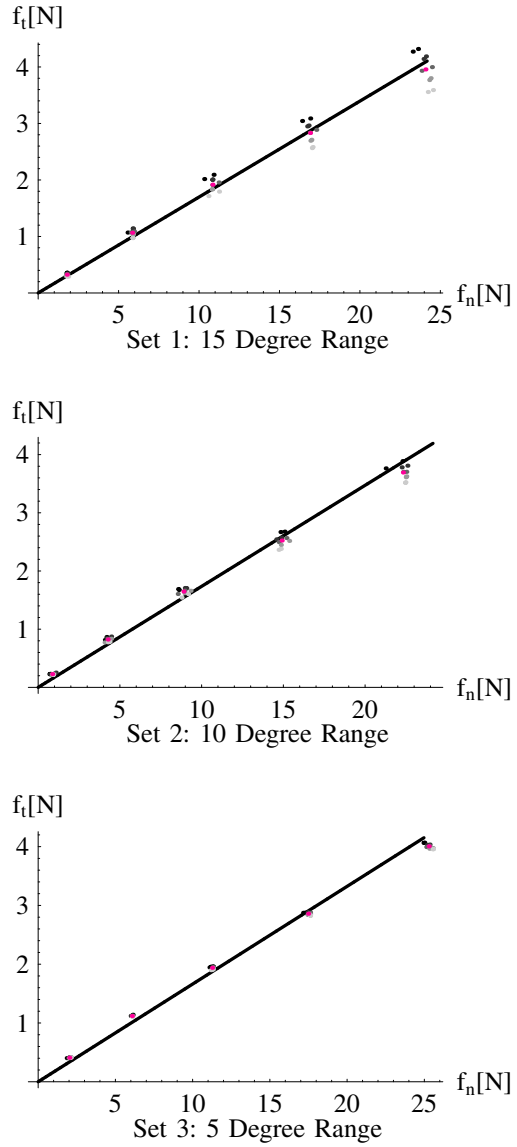

Fig. 8. Nonlinear loading path convergence point data and model fit

TABLE III

NONLINEAR LOADING PATH DISPERSION STATISTICS

	Total Err.	Mean Norm. Err.
Set 1	10.28[N]	1.8 %
Set 2	9.28[N]	3.6 %
Set 3	4.61[N]	1.0 %

the equivalent dependence of each force component on its respective displacement. Critically, *no model* which has as its only state δ_n, δ_t can predict the dispersion of the data at the convergence points, since these points are at the same position in the (δ_n, δ_t) plane. Statistics characterizing the dispersion of these points is shown in Table III. See the Appendix for a description of each statistic.

The dispersion of the data points decreases as the loading paths approach linear loading paths, as would be expected. For the large loading path variations in Set 1, the data is visibly spread apart, however, the mean normalized error, characterizing this spread is only 1.8%. This indicates that if the linear loading path model was used to predict the forces for the nonlinear loading paths at the convergence point, on average this model would only be incorrect by 1.8%. The reason for the unexpected larger mean normalized error of Set 2 is that the zero displacement changed and the experiment begun in smaller displacements and smaller forces. Therefore the means of the forces are also smaller than in the other sets, hence increasing the mean normalized error.

V. APPLICATION TO SNAKE CLIMBING

In this section we briefly sketch the application of the contact model developed here for the stability analysis of a climbing snake robot. Stability is important not only because it allows the robot to recover from a local deviation from the predefined path, but also because it allows the robot to actually move from one stable equilibrium to another.

The snake robot's configuration parameters are denoted as follows: The first link configuration (position and orientation) is denoted $\boldsymbol{q}_0 \in SE(3)$. The snake has n revolute joints. Hence, q_i represent the angle of the i^{th} joint. The full configuration of the snake is represented by $\boldsymbol{q} = (\boldsymbol{q}_0, q_1, ..., q_n)^T \in \mathcal{Q}$, where $\mathcal{Q} = SE(3) \times S^n$. In general the overall dynamics of the snake can be represented as:

$$M(\boldsymbol{q})\ddot{\boldsymbol{q}} + C(\boldsymbol{q}, \dot{\boldsymbol{q}})\dot{\boldsymbol{q}} + G(\boldsymbol{q}) = \begin{pmatrix} \mathbf{0} \\ \boldsymbol{\tau} \end{pmatrix} + \sum_{i=1}^{m} J_i^T(\boldsymbol{q}) F_i \quad (5)$$

where $M(\boldsymbol{q})$ is the snake's inertia matrix, $C(\boldsymbol{q}, \dot{\boldsymbol{q}})\dot{\boldsymbol{q}}$ represent the centrifugal and Coriolis forces, $G(\boldsymbol{q})$ is the vector of gravitational force, and m is the number of contact points between the snake and the environment. Obviously, when the i^{th} contact breaks the corresponding generalized force $J_i^T(\boldsymbol{q})F_i$ vanishes.

The first term on the right hand side of (5) contains the torques that the joints' actuators apply, $\boldsymbol{\tau}$. These joint torques are being controlled by a simple decentralized PD controller. The second term on the right hand side of (5) includes the effect of the contact forces on the dynamics of the snake. Each F_i is the i^{th} contact force vector. This contact force vector is then multiplied by the transpose of the snake's Jacobian matrix computed for the i^{th} contact point.

The compliant contact model allows us to express the contact forces as function of the corresponding displacements. The displacements are functions of the the robot's configuration. Thus the entire robot dynamics can be expressed as function of the robot's state. Thus, the robot's equation of motion is:

$$\begin{aligned} M(\boldsymbol{q})\ddot{\boldsymbol{q}} + C(\boldsymbol{q}, \dot{\boldsymbol{q}})\dot{\boldsymbol{q}} + G(\boldsymbol{q}) = & -P(\boldsymbol{q} - \bar{\boldsymbol{q}}^*) - D\dot{\boldsymbol{q}} \\ & - \textstyle\sum_{i=1}^{m} J_i^T(\boldsymbol{q}) R_i \begin{pmatrix} k_i^t \delta_i^t(\boldsymbol{q}) \sqrt{\delta_i^n(\boldsymbol{q})} \\ k_i^n \sqrt{\delta_i^n(\boldsymbol{q})} \end{pmatrix}, \end{aligned} \quad (6)$$

where $P \in I\!R^{(n+3)\times(n+3)}$ and $D \in I\!R^{(n+3)\times(n+3)}$ are the proportional gain and the damping matrices. Based on the robot's dynamic system (6) and following stability analysis tools from control theory we can obtain conditions for asymptotically stable equilibrium configurations [11]. The

control paradigm sketched here is proved to stabilize the robot both theoretically and experimentally, and a video showing the climbing snake can be downloaded from the authors website.

VI. Conclusion and Future Work

The purpose of the paper is to investigate how well a simple lumped parameter model, based on the Walton model, can be used to predict contact forces across a variety of loading paths for a single compliant material. We looked at three different types of loading paths: normal loading, linear loading, and nonlinear loading paths.

The normal loading and linear loading path data were well fit by the model form suggested by the Walton model, which postulates that normal force is proportional to $\delta_n^{\frac{3}{2}}$ and the tangential force is proportional to $\sqrt{\delta_n}\delta_t$.

The nonlinear loading experiments were used to test how large the dependence of contact forces was on loading path. To test this dependence on loading path, we looked at the dispersion of contact force data at a variety of loading path convergence points. As the loading paths approached a single linear loading path, the dispersion approached zero, which suggests that *for small deviations from a linear loading path, a path independent model should hold.* More experimental work needs to be performed to characterize the effect of the variety of nonlinear loading paths that are possible. We also showed that this model can be pluged into the snake robot's dynamic equations to form a dynamic model that depends only on the robot's state. This will allow simple stability analysis based on known tools from control theory.

In the future, we would like to extend the experiments to other compliant materials, like foam, to see the effect of different material properties. we would also like to study the affects of contact geometry, contact friction, and loading velocity on the force-displacement data. More non-linear loading path experiments are needed to fully characterize how quickly the force-displacement data becomes path dependent when we deviate from a loading profile.

Importantly, the experimental setup needs to be further improved to gather more accurate data for all future experiments. The two most serious forms of error in the current experimental setup are the axis misalignment between the force sensor and the pusher axis, and a form of creep in the experiments. The effect of creep is that the zero displacement position changes from experiment to experiment even though the compliant material has not changed position.

Appendix A: Experimental Details

A. Calibration Procedure

The force sensor Z-axis was manually aligned with the pusher axis by manipulating the clamp holding the force sensor. To test a potential direction for the force sensor, the pusher was moved along the aligned axis against the compliant material until a 25[N] force registered on the force sensor Z-axis. Ideally, no force would register on the X and Y axes, indicating that the Z-axis and the pusher axis were perfectly aligned. After calibration, we registered 0.25[N] force in the tangential (XY) plane at 25[N] Z force.

The location where the compliant material was first contacted by the pusher had to be located in order to determine displacement data. For the purposes of our experiments, we considered the 3^{rd} of three force sensor reading above a value of .03[N] to indicate the zero of the compliant material. This zero was found at the beginning of each experiment.

B. Experimental Details

Several procedural details where shared by all experiments. First, in all experiments we attempted to move in $10[\mu m]$ steps along the desired path. However, due to the the $1[\mu m]$ resolution of the NEAT device, paths which were not axis aligned suffered from discretization error. Secondly, each axis of the NEAT 310 was controlled independently. To approximate moving along a line which was not axis aligned, the NEAT device was first moves along the normal axis, and then along the tangential axis in a staircase fashion.

C. Normal and linear loading path statistics

1) R^2- coefficient of determination as reported by Mathematica ©.
2) Mean Abs. Err. - $\frac{1}{n}\sum_{i=1}^{n} \|f_{d_i} - f_{m_i}(\delta_t, \delta_n)\|$ where f_{d_i} is the i^{th} force data point, of either normal force or tangential force, f_{m_i} is the model's prediction of force, and n is the number of data points.
3) Mean Norm. Abs. Err. - $\frac{1}{n}\sum_{i=1}^{n} \|\frac{f_{d_i} - f_{m_i}(\delta_t, \delta_n)}{f_{m_i}}\|$.
4) Max Err. - $\max_i(f_{d_i} - f_{m_i})$.
5) Min Err. - $\min_i(f_{d_i} - f_{m_i})$.

D. Nonlinear loading path statistics

1) Total Err. - $\sum_i \sum_j \|(f_{n_{ij}}, f_{t_{ij}}) - (\mu_{n_j}, \mu_{t_j})\|_2$ where $(f_{n_{ij}}, f_{t_{ij}})$ is the i^{th} force data point at the j^{th} convergence point with normal and tangential component respectively and (μ_{n_j}, μ_{t_j}) is the mean force at the j^{th} convergence point.
2) Mean Norm. Err. - $\frac{1}{n}\sum_i \sum_j \frac{\|(f_{n_{ij}}, f_{t_{ij}}) - (\mu_{n_j}, \mu_{t_j})\|_2}{\|(\mu_{n_j}, \mu_{t_j})\|_2}$

References

[1] H. Hertz, "On the contact of elastic solids," *Journal of Reine and Angewandte Mathematik*, 1882.

[2] K. Walton, "The oblique compression of two elastic spheres." *Jour. of Mech. Phys. Solids*, vol. 26, pp. 139 – 150, 1978.

[3] ——, "The effective elastic moduli of arrandom packing of spheres," *J. Mech. Phys. Solids*, 1987.

[4] D. Elata, "On the oblique compression of two elastic spheres," *Journal of Applied Mechanics*, 1996.

[5] R. Mindlin, "Compliance of elastic bodies in contact," *ASME Journal of Applied Mechanics*, 1949.

[6] R. Mindlin and H. Deresiewicz, "Elastic spheres in contact under varying oblique forces," *ASME Journal of Applied Mechanics*, 1953.

[7] D. Elata and J. Berryman, "Contact force-displacement laws and the mechanical behavior or random packs of identical spheres." *Mechanics of Materials*, 1996.

[8] N. Xydas, M. Bhagavat, and I. Kao, "Study of soft-finger contact mechanics using finite elements analysis and experiments." in *Proc. IEEE Int. Conf. on Robotics and Automation*, 2000.

[9] D. Stewart, "Rigid-body dynamics with friction and impact." *SIAM Review*, 2000.

[10] J. Burdick, Y. Liang, and E. Rimon, "Experiments in fixturing mechanics," in *Proceeding of International Conference on Robotics and Automation*, 2003.

[11] A. Shapiro, "Design and control of an autonomous spider-like robot for motion in 2d tunnel environments." Ph.D. dissertation, Technion-Israeli Institue of Technology, 2003.